Article

Prebiotic Xylo-oligosaccharides Targeting *Faecalibacterium prausnitzii* Prevent High Fat Diet-induced Hepatic Steatosis in Rats

Sanna Lensu[1], Raghunath Pariyani[2], Elina Mäkinen[1], Baoru Yang[2], Wisam Saleem[3], Eveliina Munukka[4,5], Maarit Lehti[1], Anastasiia Driuchina[1], Jere Lindén[6], Marja Tiirola[7], Leo Lahti[3], and Satu Pekkala[1,5]*

[1] Faculty of Sport and Health Sciences, University of Jyväskylä, Jyväskylä, Finland; sanna.t.k.lensu@jyu.fi; elina.e.makinen@jyu.fi; maarit.t.lehti@jyu.fi; anastasiia.a.driuchina@jyu.fi; satu.p.pekkala@jyu.fi
[2] Food Chemistry and Food Development, Department of Biochemistry, University of Turku, Turku, Finland; raghunath.pariyani@utu.fi; bayang@utu.fi
[3] Department of Future Technologies, University of Turku, Turku, Finland; wisam.tariqsaleem@utu.fi; leo.lahti@utu.fi
[4] Institute of Biomedicine, University of Turku, Turku, Finland; laevmu@utu.fi
[5] Department of Clinical Microbiology, Turku University Hospital, Turku, Finland
[6] Veterinary Pathology and Parasitology, University of Helsinki, Helsinki, Finland; jere.linden@helsinki.fi
[7] Department of Environmental and Biological Sciences, University of Jyväskylä, Jyväskylä, Finland; marja.tiirola@jyu.fi
* Correspondence: satu.p.pekkala@jyu.fi; Tel.: +358-45-358-28-98 (S.P.)

Abstract: Understanding the importance of gut microbiota (GM) in non-alcoholic fatty liver disease (NAFLD) has raised the hope for therapeutic microbes. We have shown that high hepatic fat associated with low abundance of *Faecalibacterium prausnitzii* in humans and further, administration of *F. prausnitzii* prevented NAFLD in mice. Here, we aimed to target *F. prausnitzii* by prebiotic xylo-oligosaccharides (XOS) to treat NAFLD. First, the effect of XOS on *F. prausnitzii* growth was assessed *in vitro*. Then, XOS was supplemented or not with high (HFD) or low (LFD) fat-diet for 12-weeks in Wistar rats (n=10/group). XOS increased *F. prausnitzii* growth having only minor impact on the GM composition. When supplemented with HFD, XOS prevented hepatic steatosis. The underlying mechanisms involved enhanced hepatic β-oxidation and mitochondrial respiration. ^{1}H-NMR analysis of caecal metabolites showed that compared to HFD, LFD group had healthier caecal short-chain fatty acid profile and the combination of HFD and XOS was associated with reduced caecal isovalerate and tyrosine, metabolites previously linked to NAFLD. Caecal branched-chain fatty acids associated positively and butyrate negatively with hepatic triglycerides. In conclusion, our study identifies *F. prausnitzi*i as a possible target to treat NAFLD with XOS. The underlying preventive mechanisms involved improved hepatic oxidative metabolism.

Keywords: prebiotic; oligosaccharides; gut microbiota; fatty liver; metabolism; mitochondria

1. Introduction

In Western countries, nearly 30% of the general population and up to 90% of obese individuals suffer from non-alcoholic fatty liver disease (NAFLD) [1]. NAFLD is defined as excessive fat accumulation in liver without the patient having secondary causes of fat accumulation, such as excessive drinking of alcohol or use of steatogenic drugs. NAFLD can be categorized into simple hepatic steatosis, which is diagnosed as a presence of fat accumulation without histological or biochemical injuries, and non-alcoholic steatohepatitis (NASH), characterized by hepatic steatosis, inflammation and hepatocyte damage [2, 3].

It is increasingly accepted that the pathogenesis of NAFLD is associated with environmental, host genetic and physiological factors [4], such as increased lipid storage [5-7] and mitochondrial

Preprints (www.preprints.org) | NOT PEER-REVIEWED | Posted: 11 September 2020 doi:10.20944/preprints202009.0241.v1

dysfunction [7]. Often, dietary factors and excessive caloric intake are involved in pathogenesis of NAFLD, and they are also important determinants of the gut microbiota (GM) composition of the host [8]. The GM refers to the trillions of tiny microbial cells inhabiting the gastrointestinal tract that brake down the macromolecules and nutrients from the ingested food. Complex interactions between dietary factors and microorganisms are known to dictate the beneficial or detrimental effects on the host health [8]. Prominently, recent studies have highlighted the importance of gut-derived signals [9, 10] and the entity of the GM in the pathogenesis of NASH and NAFLD. In NAFLD patients, for instance over-represented *Gammaproteobacteria* [11, 12] and the genera *Lactobacillus*, *Dorea*, *Robinsoniella* and *Roseburia* [13] have been found compared to healthy controls. Controversially, either low abundance [14] or high abundance [15] of the phylum *Bacteroidete*s have been detected in NASH patients. Another study reported enriched *Fusobacteria*, *Lachnospiraceae, Enterobacteriaceae*, *Erysipelotrichaceae* and *Streptococcaceae* in NAFLD patients [16]. These studies indicate that there is no single microbial taxon always positively or negatively associated with liver fat, which, however, may be influenced by the age, gender and geographic location of the study cohorts that are known to affect the GM composition [17-20].

The involvement of the GM in NAFLD has led to the development of possible therapies that either use health-beneficial microbes or target the GM of the host. We have shown that intragastric administration of *Faecalibacterium prausnitzii*, a commensal member of the GM with known anti-inflammatory properties [21, 22], prevented NAFLD in mice [23]. The rationale for investigating this bacterium in the mice model stemmed from our human study, which showed that *F. prausnitzii* abundance associated reversely with hepatic fat content [24], and thus we hypothesized that its low abundance might partly contribute to the diseased phenotype. Our study was in agreement with another study that detected under-represented *F. prausnitzii* in NASH patients [25].

Our previous findings thus tentatively suggested that NAFLD might be partly relieved with *F. prausnitzii.* Unfortunately, the potential "therapeutic" bacteria are not always accepted for human use. We therefore searched alternative, nutrition-based tools to increase the natural abundance of *F. prausnitzii* to treat NAFLD. Such effective tools are known to be probiotics and prebiotics, for instance [26]. A probiotic refers to a live microorganism that confers health benefits to the host, while a prebiotic is defined as a selectively fermented component that cannot be digested as such but serves as a food for the GM and thereby causes specific changes in the composition and/or activity of GM conferring beneficial effects for host's health. Carbohydrates, such as dietary fibre, are potential prebiotics. These include fructooligosaccharides (FOS), galactooligosaccharides (GOS), isomaltooligosaccharides (IMO), xylooligosaccharides (XOS), transgalactooligosaccharides (TOS), and soybean oligosaccharides (SBOS) [26]. Previously, a high dose of XOS that is isolated from corncobs, 2.8 grams daily - that may not actually be considered as prebiotic dose - has been shown to increase the abundance of *Faecalibacterium* species in a group of seven healthy humans [27]. On a contrary, two *in vitro* studies failed to show any stimulatory effect of XOS on *F. prausnitzii* growth [28, 29]. Moreover, a human study did not show effects of XOS on *F. prausnitzii* but a slightly improved glucose tolerance was achieved in pre-diabetic subjects, when they consumed 2 grams of XOS daily, for eight weeks [30].

In this study, we tested the effect of a prebiotic dose of XOS (0.12% w/v) on enhancing *F. prausnitzii* growth first *in vitro,* and then *in vivo*. In rats, NAFLD was induced with high-fat diet (HFD), with or without XOS supplementation. In addition, the effects of XOS (or not) were studied in healthy controls, i.e. in normal, low-fat diet (LFD) fed counterparts that did not generate NAFLD.

2. Materials and Methods

Preprints (www.preprints.org) | NOT PEER-REVIEWED | Posted: 11 September 2020 doi:10.20944/preprints202009.0241.v1

2.1. In vitro cultivations of Faecalibacterium prausnitzii

In vitro cultivations of *F. prausnitzii* were done in fastidious anaerobe broth (FAB) supplemented with short-chain fatty acids (SCFA) in an anaerobic workstation (WhitleyA35, Don Whitley Scientific, West Yorkshire, UK). The effects of XOS were studied on two commercially available *F. prausnitzii* strains; ATCC®-27766™ (Manassas, VA, USA) and DSM A2-165 (Braunschweig, Germany), with three replicates for both. Ten ml cultures of FAB+SCFA media were supplemented or not with XOS as 0.5 % (w/v %). XOS was isolated from corncobs (*Zea mays* subsp. *mays*) *via* enzyme-catalyzed hydrolysis and subsequent purification. It was donated by the manufacturer Shandong Longlive Biotechnology LTD, China (95 % pure, CAS #87099-0). The growth of *F. prausnitzii* was determined by following changes in the optical density at 620 nm with MultiskanFC photometer (Thermo Fisher Scientific, Waltham, MA, USA) after 22 hours of cultivations.

2.2. Animals

The animal experiment was approved by the National Animal Experiment Board of Southern Finland (ESAVI/8805/4.10.07/2017), and performed in accordance with the Guidelines of the European Community Council directives 2010/63/EU, and European Convention for Protection of Vertebrate Animals used for Experimental and other Scientific Purposes (Council of Europe No123, Strasbourg 1985). It was conformed according to the Animal Research: Reporting of *In Vivo* Experiments (ARRIVE) guidelines. Male Wistar rats of 10-12 weeks old were purchased from Charles River, Europe. Wistars were chosen because our pilot studies indicated that they harbour *F. prausnitzii* while Sprague Dawley for instance, did not (data not shown). Upon arrival, the rats were let to habituate to the environment for two weeks. During the whole experiment, the rats were single-housed. The animals were randomly divided into four groups (n=10/group): 1) High-fat diet (HFD, with 60% of energy from fat), 2) HFD supplemented with XOS (0.12%, HFD+XOS), 3) control = low-fat diet (LFD, with 10% of energy from fat), and 4) LFD supplemented with XOS (0.12%, LFD+XOS). It is of note, that control feed contained standard amount of fat available in rodent feed, but for clarity and big difference to the high-fat group it is termed LFD. In humans, a daily dose of around one gram of XOS yields prebiotic effects. Thus, in rats taking into account that animal weighs around 100-times less than humans, 0.12% of XOS used in this study can be considered as a safe prebiotic concentration. XOS was isolated as described above and donated by Shandong Longlive Biotechnology (95% pure, CAS #87099-0). All irradiated diets were purchased as custom-made pellets from Labdiet/Testdiet, UK. The animals had food and water *ad libitum* and were maintained at 12/12h light/dark cycle in an enriched environment at animal facilities of University of Jyväskylä. At the beginning of the 12-week diet intervention all rats were ~15 weeks of age.

2.3. Indirect metabolic measurements

The indirect measures of metabolism were analyzed from respiratory gases with oxygen, CO_2 and capacitive water vapor partial pressure analyzer (Promethion®GA3, Sable Systems, Las Vegas, NV, USA). Two multi-channel mass flow generators measured and controlled air flow (FR8, Sable Systems). The incurrent flow rate was 3500 mL/min. The data acquisition was coordinated by MetaScreen® and the raw data were processed using ExpeData® softwares (Sable Systems). Expedata uses an analysis script detailing all aspects of data transformation, calculates respiratory quotient (RQ) as the ratio of CO_2 production over O_2 consumption, and energy expenditure using the Weir equation: $Kcal/hr=60*(0.003941*VO_2+0.001106*VCO_2)$ [31].

2.4. Weight and body composition measurement, food intake

Preprints (www.preprints.org) | NOT PEER-REVIEWED | Posted: 11 September 2020 doi:10.20944/preprints202009.0241.v1

During the study the animals were weighed weekly always at the same time of day on an electronic scale. The food intake was measured once a week by weighing the consumed feed during 24-hours. The body composition was determined with dual energy x-ray absorptiometry (DXA, Prodigy; GE Lunar Corp., Madison, WI, USA) under isoflurane anesthesia before and after the diet intervention.

2.5. Necropsy, blood analyses, tissue collection and histology

After the 12-week diet intervention, the non-fasted rats were anesthetized with a mixture of air and CO_2, and euthanized by drawing the blood by cardiac puncture. Serum glucose, triglycerides, free fatty acids, glycerol, cholesterol, LDL, HDL, AST, and ALT were determined using KONELAB 20XTi analyser (Diagnostic Products Corporation, Los Angeles, CA, USA). Serum cytokines were analyzed with 9-plex cytokine ELISA kit (#110449RT) according to the manufacturer's instructions using Quansys and Q-View software (Quansys Biosciences, Logan, UT, USA). The detection limits for the cytokines were as follows: interleukin (IL)-1a, 8.55 pg/ml; IL-1β, 3.58 pg/ml; IL-2, 2.74 pg/ml; IL-4, 0.45 pg/ml; IL-6, 1.4 pg/ml; IL-10, 0.26 pg/ml; IL-12, 0.41 pg/ml; interferon (IFN)-γ, 33.71 pg/ml, and tumor necrosis factor (TNF)-α, 2.72 pg/ml.

The medial lobe of the liver was harvested and after excising samples for mitochondrial respiration analysis and histology, the rest of the medial lobe was immersed in liquid nitrogen and stored at -80ºC. For the subsequent enzyme activity and fat content analyses, liver was pulverized in liquid nitrogen. For histology, liver was snap-frozen in cooled isopentane (-150ºC) and stored at -80°C. Neutral lipids were visualized from 10 µm cryosections by Oil Red O staining. Paraformalin-fixed sections were rinsed with H_2O, stained for 15 minutes with freshly prepared Oil Red O solution (Merck, Kenilworth, NJ, USA), and rinsed with 60% isopropanol to avoid over-staining. The sections were counterstained with Mayer's hematoxylin and scanned with NanoZoomer microscope (Hamamatsu, Japan). The amount of hepatic fat was scored by two blinded experimenters.

For the histology of the gut, ~10 mm of proximal colon was cut right after the caecum, the colon contents were collected (see below) and the rests were washed out with PBS. The tissue was fixed with 4% paraformaldehyde for 48 hours, washed twice with PBS and stored in 70% ethanol at +4°C. Gut sample was divided into ~2 mm pieces, which were embedded in the same paraffin block. 3 µm sections were deparaffinized, boiled in 0.01 M sodium citrate (pH 6.0) for antigen retrieval and blocked with 10% goat serum. The intestinal tight junctions were stained with anti-tight junction protein-1 antibody (Tjp1, Novus Biologicals, Littleton, CO, USA), and visualized by labeling with anti-rabbit 647 Alexa Fluor (Invitrogen, Carlsbad, CA, USA). Nuclei were imagined with DNA-stain 4',6-diamidino-2-phenylindole (DAPI, 1:2000), and sections were cover-slipped with Mowiol-mounting media. The labeled sections were imaged with confocal microscope (Carl Zeiss LSM 700) and the signal intensities were counted with Image J. From each rat, four randomly selected areas were imagined, four tiles per area (1184 µm x 1184 µm).The fluorescence intensity was normalized to the amount of DAPI intensity.

2.6. Collection of gut contents, DNA extraction and real-time quantitative PCR

Proximal colon and caecum contents were collected at necropsy, snap-frozen in liquid nitrogen and stored at -80°C. The total DNA was extracted from ~100 mg of the colon and caecum contents with Stool Extraction Kit and semi-automated GenoXtract (Hain Lifescience GmbH, Germany), combined with preceding homogenization and bead-beating in 1.4 mm Ceramic Bead Tubes.

Real-time quantitative PCR (qPCR) was performed using DNA extracted from caecum and *F. prausnitzii* 16S rRNA–targeted primers as described previously [32]. First, traditional PCR was performed using pure cultures of *F. prausnitzii* and *F. prausnitzii* 16S rRNA –targeted primers. The PCR program consisted of pre-incubation at 95ºC for 10 minutes, 40 cycles at95ºC for 30 seconds, 60ºC for 1 min and 72ºC for 30 seconds and then a final extension at 72ºC for eight minutes (Veriti 96 Well Thermal Cycler, Applied Biosystems, USA). The expected size of the PCR product was 140 base pairs. After obtaining and purifying the PCR products, a dilution series

Preprints (www.preprints.org) | NOT PEER-REVIEWED | Posted: 11 September 2020 doi:10.20944/preprints202009.0241.v1

for the qPCR standard curve was made from the pool of positive reaction products of the traditional PCR. The DNA concentration of the DNA pool was measured with NanoDropND-1000 spectrophotometer (ND, Nanodrop Technologies Inc., Wilmington, DE, USA). Assuming that the molecular weight of one DNA base pair is 660 g/mol and knowing the PCR product size to be 140 base pairs, the concentration of DNA fragments in the pool could be calculated based on the DNA concentration: DNA concentration (ng/µl)/molecular weight of one PCR fragment (g/mol)= fragment concentration. When the fragment concentration (mol/µl) was multiplied with Avogadro's number (6.0221415 × 1023), the number of fragments per one µl was gained. From this, a dilution series from 10^{10} to 10^{1} was done and used as a standard curve in the qPCR. The qPCR results are shown as *F. prausnitzii* gene copy number/gram of caecal content. However, it should be noted that the gene copy number does not directly represent the absolute *F. prausnitzii* bacterial cell numbers of the samples, because it is not known how many gene copies of 16S rRNA exist in a single *F. prausnitzii* cell.

2.7. 16S rRNA gene sequencing and processing of the sequence data

For microbial community analysis, rRNA gene was amplified using primers 515F-Y (GTGYCAGCMGCCGCGGTAA) and 806R (GGACTACHVGGGTWTCTAAT) targeting the V4 region of the SSU rRNA gene. In the first PCR, the reaction consisted of 1xMaxima™ SYBR Green qPCR Master Mix (Thermo Fisher Scientific, Waltham, USA), 0.5 µM of primers and 20 ng of DNA template. Thermal cycling consisted of 10 min initial denaturation at 95°C, 30 cycles at 94°C 30 sec, +52°C 60 s and 72°C 60 s and final extension at 72°C for 5 min (C1000 ThermalCycler, Bio-Rad Laboratories, Hercules, USA). To add Ion Torrent PGM sequencing adapters and barcodes to the ends of the PCR product, one µl of the PCR product was used as template in the second PCR, where 10 cycles were performed using linker and fusion primers (0.05 µM of M13_515F-Y, 0.5 µM of IonA_IonXpressBarcode_M13 and P1_806R), with conditions otherwise identical to the first amplification. Sequencing was performed using Ion Torrent PGM (Thermo Fisher Scientific, Waltham, USA). PCR products were purified with AMPure XP (Beckman Coulter, Brea, USA), quantified with PicoGreen (Quant-iT™ PicoGreen™ dsDNA Assay Kit, Thermo Fisher Scientific, Waltham, USA), and pooled in equimolar quantities for sequencing on Ion Torrent PGM using Hi-Q View OT2 Kit for emulsion PCR, Hi-Q View Sequencing Kit for the sequencing reaction, and Ion 318 Chip v2 (Thermo Fisher Scientific).

The 16S rRNA gene sequences were quality-filtered and clustered to operational taxonomic units (OTUs) at the 97% similarity using CLC Microbial Genomics Package (Qiagen, Germany). After processing, the data-set contained 5.0 million reads, on average 64544±15932 reads per sample and 12700 unique OTUs. The rRNA gene sequences were classified using SILVA SSU Ref database (v132, 99%). First, the GM diversity was analyzed separately from caecal and colon contents. Because no differences in the distribution of evenness between species *i.e.* alpha-diversity of the GM were observed between the two intestinal compartments (See Results, section 3.2), the sequence data of the caecum and colon samples were pooled for further GM composition analyses.

2.8. Extraction, identification and analyses of caecal metabolites

Ice-cold PBS (pH 7.4) was mixed with the caecal content at a ratio of 1:2, and vortexed for 5 min to extract caecal metabolites. The extract was then centrifuged at 15,000 × *g* for 15 min at +4°C. An aliquot of the supernatant was mixed with 10% Chenomx standard solution [5 mM deuterated DSS (DSS-d6) and sodium azide in D_2O] and vortexed for 15s. Then, 180 µL of the solution was placed into 3mm NMR-tubes. The spectra were recorded using 600 MHz Bruker AVANCE-III NMR spectrometer equipped with TCI Prodigy CryoProbe (Bruker BioSpin AG, Fällanden, Switzerland).

NMR spectra were recorded using a 600 MHz Bruker AVANCE-III NMR spectrometer (Bruker BioSpin AG, Fällanden, Switzerland) equipped with a TCI Prodigy CryoProbe. A 128 scans Carr-Purcell-Meiboom-Gill sequence (CPMG) pulse was applied to acquire the spectra consisting of 128 k data points at a spectral width of 10 kHz, at 25°C, with an acquisition time of 6.82 s. The

 doi:10.20944/preprints202009.0241.v1

parameters used in acquiring *J*-resolved (JRES) spectra were 16 scans, 1 k data points, 128 increments, 2s relaxation delay and a spectral width of 16 ppm in dimensions. The heteronuclear single quantum coherence (HSQC) spectra were acquired using 32 scans, 2 k data points, 128 increments, 2s relaxation delay, and spectral width of 16 ppm and 165 ppm in the proton and carbon dimensions, respectively.

The identification and quantification of the metabolites were performed using the metabolite library of the Chenomx NMR Suite 8.3 Professional (Chenomx Inc., Edmonton, Alberta, Canada). In addition, literature as well as open access web based metabolite databases such as Human Metabolome Database (HMDB, http://www.hmdb.ca), and Biological Magnetic Resonance data Bank (BMRB, http://www.bmrb.wisc.edu) were also queried. The metabolite identities were duly confirmed by two-dimensional NMR experiments such as JRES and HSQC.

2.9. Processing of the caecal metabolite data and multivariate data analysis

All raw ^{1}H-NMR spectra were processed individually to correct the phasing, baseline, and shim using Chenomx NMR Suite. All the spectra were referenced to the internal standard (TSP) at 0.00 ppm. The chemical shift region 0.0–10.0 ppm was then integrated to bins of width 0.001 ppm after total area normalization, using the Chenomx software. This dataset comprising of 10,000 bins was used to correct the misalignments of the spectra using the icoshift algorithm, in MATLAB platform, based on the correlational shifting of spectral intervals. The average spectrum twice (average2) was used as the target spectrum to realign the misaligned peaks. The spectral region related to residual water (4.68–4.88) and the regions lacking signals such as δ 0.0–0.6 and δ 9.5–10.0 were removed from the aligned spectra. The newly constructed aligned binned data was reduced to variable sized bins of size ranging from 0.018 – 0.04 ppm.

The generated dataset comprising 40 observations and 157 variables was then used in the multivariate data analysis using SIMCA-P 14.1 (Umetrics, Sartorius Stedim Biotech, Umeå, Sweden). The mean centered and Pareto scaled data was subjected to unsupervised principal component analysis (PCA) and supervised Partial Least Squares-Discriminant Analysis (PLS-DA) and/or Orthogonal Partial Least Squares-Discriminant Analysis (OPLS-DA). The grouping patterns of the samples in different chemometric analysis were observed with the aid of score plots, wherein the spectra were represented as individual points along the principal components. The variables (metabolites) contributing to the characteristic grouping of the samples observed in the score plots were visualized using their corresponding loading plots. The validation as well as the evaluation of the optimal fit of the OPLS-DA models were performed by internal validation methods of 100 permutation test, calculation of explained variation (R2Y (cum)), predictive ability (Q2Y (cum)), and CV-ANOVA values.

2.10. Measurement of liver fat content and 3-hydroxyacyl-CoA dehydrogenase activity

Total lipids were extracted from pulverized sample of the medial lobe of liver and analyzed with KONELAB 20XTi as described previously [33]. To analyze the activity of 3-hydroxyacyl-CoA dehydrogenase 8 (β-HAD), ~20 mg of pulverized livers were homogenized in ice-cold lysis buffer (10 mM Tris-HCl, 150 mM NaCl, 2 mM EDTA, 1% Triton X-100, 10% glycerol and 1 mM DTT), supplemented with protease and phosphatase inhibitors (Sigma Aldrich, St Louis, USA) using TissueLyzer (Qiagen, Valencia, CA, USA). After centrifugation at 12.000 x *g*, β-HAD activity was measured with KONELAB 20XTi in a solution containing 50 mM Triethanolamine-HCl (pH 7.0), 4 mM EDTA, 0.04 mM NADH and 0.015 mM S-Acetoacyl CoA.

2.11. Measurement of hepatic mitochondrial functions with high-resolution respirometry reflecting the rate of hepatic glucose metabolism

Preprints (www.preprints.org) | NOT PEER-REVIEWED | Posted: 11 September 2020 doi:10.20944/preprints202009.0241.v1

Freshly collected sample of liver medial lobe (15-20 mg) was homogenized in 0.5 ml Mir05-medium with PBI-Schredder HRR set (Oroboros instruments, Innsbruck, Austria). Shredding was done 10 s 1-level + 5 s 2-level. Shredding pipe was washed three times with 0.5 ml of Mir05-medium and collected to clean tube with the homogenate. The final volume of the homogenate was set to 5 ml with Mir05-buffer. An aliquot of 0.8 ml of the homogenate and 1.5 ml of Mir05-medium were transferred to the Oroboros O2k-Respirometer (Oroboros instruments). Oxygen concentration (μM), and oxygen flux per tissue wet mass (pmol O2•s−1•mg−1) were recorded using DatLab software (Oroboros instruments). Oroboros program was performed as follows: 1) Pyruvate, malate, and glutamate (5 mM, 2 mM, 10 mM) were used as initial substrates but without ADP leak-respiration was measured. 2) Addition of ADP and Mg^{2+} (4 mM, 2.4 mM) started oxidative phosphorylation through mitochondrial complex I (CI). 3) Cytochrome c (10 μM) was added in order to monitor unwanted mitochondrial degradation; 4) Succinate (10 mM) was added as a complex II substrate (CI+II). 5) Maximal capacity of electron transport system was measured adding CCCP (0.5-2.5 μM; until max O_2 consumption was reached). 6) Complex I was inhibited with rotenone (0.5 μM) and 7) complex III with antimycin A (2.5 μM) and only residual oxygen consumption (ROX) was left. ROX was subtracted from all other oxygen flux values and values were expressed as normalized to wet tissue mass.

2.12. Statistical analyses

Statistical analyses, except for the gut microbiota and their metabolites, were done using IBM SPSS Statistics v24 for Windows (SPSS, Chicago, IL, USA). The main effects of diet and XOS were determined using general linear model or mixed model analysis. The group differences were analyzed with ANOVA. Kruskal-Wallis test was used if the data were not normally distributed according to Shapiro Wilk's test. For the repeated measures, we used linear mixed model. Type III tests of fixed effects with Sidak's adjustment for multiple comparisons were used. Cohen's *d* was used to estimate differences between the groups in *F. prausnitzii* abundance because of the high inter-individual variation. The associations between the variables were studied with Spearman correlation coefficient.

The alpha-diversity of the GM was quantified with Shannon index using *microbiome* R/Bioconductor package. Beta-diversity analysis was based on Bray-Curtis distance and PERMANOVA [34] for significance testing (*adonis* function in the *vegan* R package). The taxonomic groups were compared based on DESeq2 [35] using *phyloseq* R/Bioconductor package including Benjamini-Hochberg correction for multiple testing. The statistical significance was set at $p < 0.05$ after the multiple testing corrections.

The univariate analysis of the concentrations of caecal metabolites was performed using Graph Pad Prism 8.0 (GraphPad Software, San Diego, CA). Normal distribution of the data was tested with the Shapiro–Wilk test. The differences between groups were assessed with the parametric one way ANOVA (normally distributed variables) with Tukey's multiple comparison test or non-parametric Kruskal-Wallis test (non-normally distributed variables) with Dunn's multiple comparisons. The statistical significance was determined at $p < 0.05$.

3. Results

3.1. XOS increased the growth of Faecalibacterium prausnitzii and concomitantly decreased hepatic fat content due to enhanced fat and glucose metabolism

Compared to the control treatment, XOS increased [$F(1, 8) = 145.6$, $p < 0.001$] the growth of *F. prausnitzii* ATCC-27766 strain ($p = 0.004$) and of DSM A5-165 strain ($p < 0.001$) *in vitro* after 22 h of stimulation (Figure 1a).

In rats, after 12-weeks of dietary XOS supplementation, *F. prausnitzii* abundance increased compared to the HFD (Cohen's *d*=0.2) and LFD (Cohen's *d*=0.2) without XOS (Figure 1b). Real-time quantitative

Preprints (www.preprints.org) | NOT PEER-REVIEWED | Posted: 11 September 2020 doi:10.20944/preprints202009.0241.v1

PCR was used to analyze *F. prausnitzii* abundance, because unfortunately, the primers used in 16S rRNA gene sequencing did not catch *F. prausnitzii*.

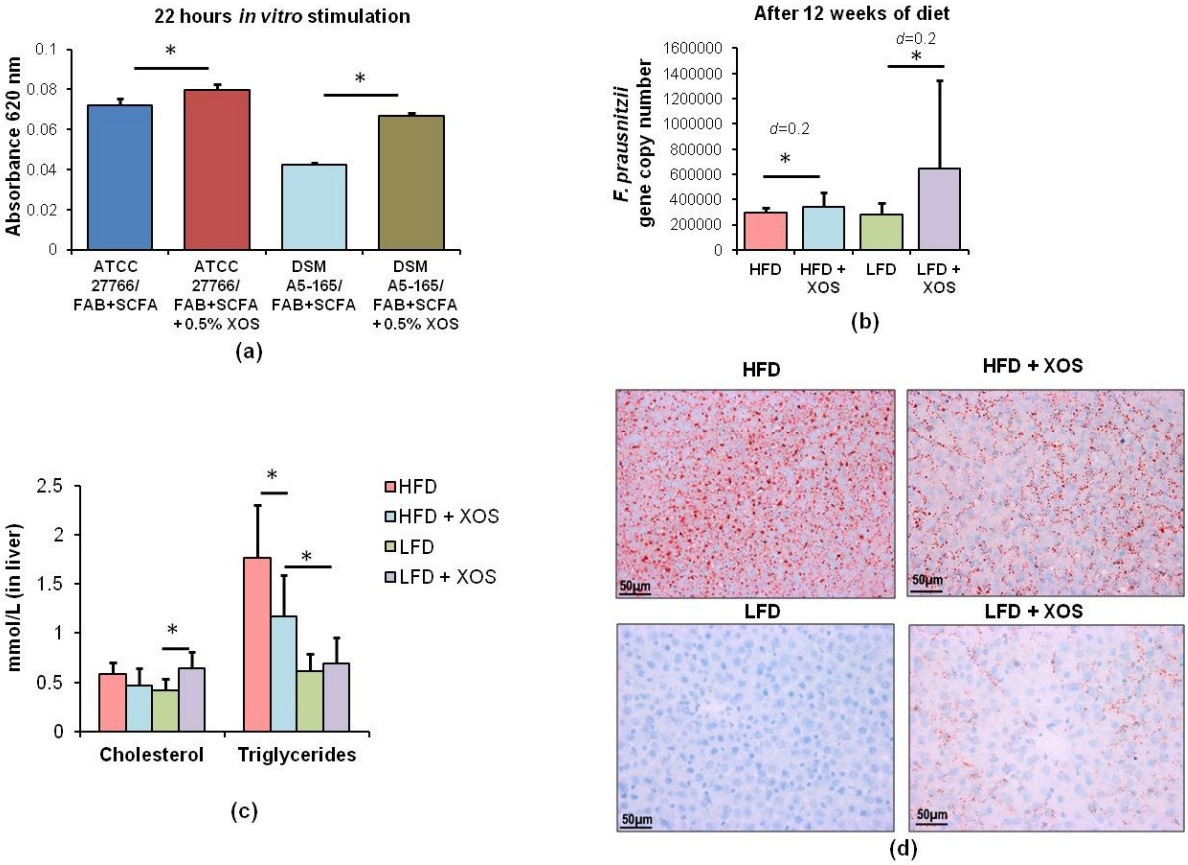

Figure 1. XOS increased the growth of *F. prausnitzii in vitro* and *in vivo* decreasing concomitantly hepatic fat content. (**a**) *In vitro* stimulation of *F. prausnitzii* growth with XOS. Cultivations of *F. prausnitzii* were done in fastidious anaerobe broth (FAB) supplemented with short-chain fatty acids (SCFA) in anaerobic workstation for 22 hours. 10 ml cultures of commercially available *F. prausnitzii* strains ATCC®-27766™ and DSM A2-165 were supplemented or not with XOS as 0.5% (w/v%). The growth of *F. prausnitzii* was determined by following changes in the optical density at 620 nm; (**b**) Quantitative real-time PCR of *F. prausnitzii* using DNA extracted from rat cecum after 12-weeks of diet. The results are shown as gene copy number divided per gram of caecum content used to extract the total bacterial DNA. Cohen's *d* was used to estimate the differences between the groups; **(c)** Biochemical analyses of total hepatic cholesterol and triglycerides; **(d)** Frozen liver sections of rats after the 12-weeks diet intervention stained with Oil Red O. The scale bar is 50 µM. The histological images were taken with Olympus BX50 microscope and Colorview III camera using 40 x objective (Olympus, NA 0.75). * indicates statistically significant difference between the groups.

The biochemical measurement of hepatic triglyceride content showed that HFD increased triglycerides [F (1, 6.0) = 46.4, p < 0.001). The interactive effect of XOS was significant [F (1, 0.8) = 6.5, p = 0.017] *i.e.* with HFD XOS decreased triglycerides while with LFD XOS increased triglycerides (Figure 1c). Similar interactive effect of XOS was found on hepatic cholesterol [F(1, 0.2) = 15.2, p = 0.001], XOS decreased it with HFD while with LFD cholesterol level was increased, although in group comparisons only the LFD+XOS had significantly higher cholesterol content than the LFD group (p= 0.015, Figure 1c). To confirm the findings on hepatic triglycerides, the medial lobe of the liver was analyzed also histologically. Oil Red O -staining of the frozen sections showed that XOS supplementation was associated with decreased hepatic neutral lipids compared to the HFD in rats (Figure 1d). To assess whether the decreased hepatic fat content was due to increased fat oxidation,

Preprints (www.preprints.org) | NOT PEER-REVIEWED | Posted: 11 September 2020 doi:10.20944/preprints202009.0241.v1

we determined the activity of β-HAD, the rate-limiting enzyme of fatty acid β-oxidation. XOS increased hepatic activity of β-HAD significantly [F (1, 2.46) = 4.74, p = 0.038, Figure 2a].

We then analyzed hepatic glucose metabolism using high-resolution respirometry. In the hepatic mitochondria, HFD had lower maximal electron transport compared to the LFD (p=0.034) that was not seen in the HFD+XOS (Figure 2b). The HFD had also lower maximal electron transport capacity theoretically available for oxidative phosphorylation (p=0.023), and the reserve electron transport capacity beyond the oxidative phosphorylation through complex I (p=0.019) as well as complexes I and II (p=0.013) than the LFD (Figure 2c). When supplemented with XOS, this effect of HFD was not observed (Figure 2c). Compared to the HFD, HFD+XOS had increased respiratory capacity available for ATP production through electron flow from complex I (p=0.023, Figure 2c) and improved coupling of electron transport through complex I and oxidative phosphorylation (p=0.041, Figure 2d).

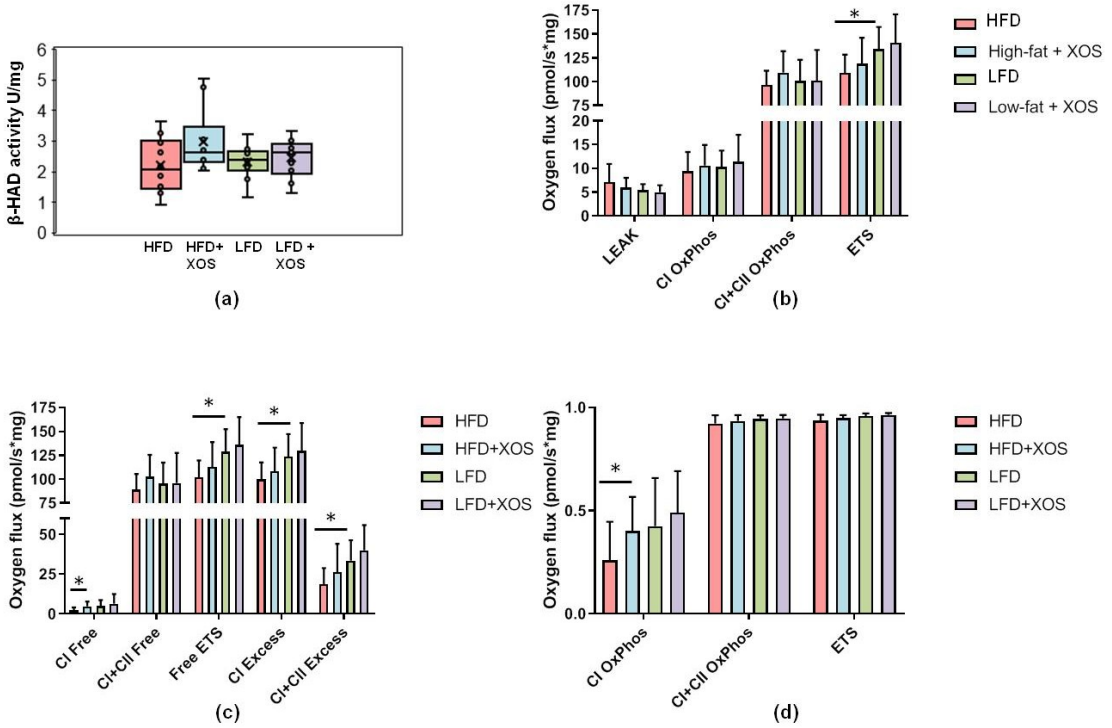

Figure 2. XOS enhanced hepatic activity of fatty acid-oxidating β-HAD and mitochondrial respiration reflecting increased glucose metabolism. (a) Biochemically measured activities of β-HAD in rat livers; **(b)** HFD had lower maximal electron transport (ETS) in liver compared to the LFD; **(c)** Compared to the LFD, HFD had lower maximal electron transport capacity available for oxidative phosphorylation (Free ETS), reserve electron transport capacity beyond oxidative phosphorylation through complex I (CI Excess) as well as through complexes I and II (C+CII Excess). Compared to the HFD, XOS increased respiratory capacity available for ATP production through electron flow from complex I (CI Free); **(d)** Compared to the HFD, XOS improved coupling of electron transport through complex I and oxidative phosphorylation (CI OxPhos, coupling efficiency). * indicates statistically significant difference between the groups.

3.2. The diets did not affect the diversity of the gut microbiota, but minor differences were found in the relative abundances of the microbial genera

Despite the over 12000 OTUs, the proximal colon and caecum of the rats were dominated by a few phyla and genera. *Bacteroidetes* (51.6% of all sequences) and *Firmicutes* (39.7%) were the dominating bacterial phyla, followed by *Verrucomicrobia* (3.6%) and *Proteobacteria* (2.3%). The families *Tannerellaceae* (19.1%, only genus *Parabacteroides*), *Rikennellaceae* (14.6%, mostly genus

Preprints (www.preprints.org) | NOT PEER-REVIEWED | Posted: 11 September 2020 doi:10.20944/preprints202009.0241.v1

Alistipes) and *Muribaculaceae* (10.0%, several genera) explained the dominance of *Bacteroidetes*, and the families *Ruminococcaceae* (16.4%), *Lachnospiraceae* (13.3%) were dominating the sequences belonging to *Firmicutes*. The hierarchical clustering analysis suggested two main clusters among the rat groups based on their GM profiles. The dietary fat explained the clusters regardless of XOS supplementation (data not shown). However, the diets did not affect the alpha-diversity of the colon or caecum GM (Figure 3a) or the beta-diversity (Figure 3b). The GM composition did not differ between the groups at phylum (Figure 4a) or family level, including *Ruminocaccaceae* family to which *F. prausnitzii* belongs (data not shown). At genus level, *Dubosiella* and uncultured member of *Christensenellaceae* were lower, and *Prevotellacaeae* NK3B31 group higher in the HFD+XOS (p=0.01 for all, Figure 4B). The microbiota of the HFD tended to have higher relative abundance of *Prevotellacaeae* UCG-10 (p=0.06), and LFD groups higher abundance of *Anaerostipes* (p=0.10) (data not shown).

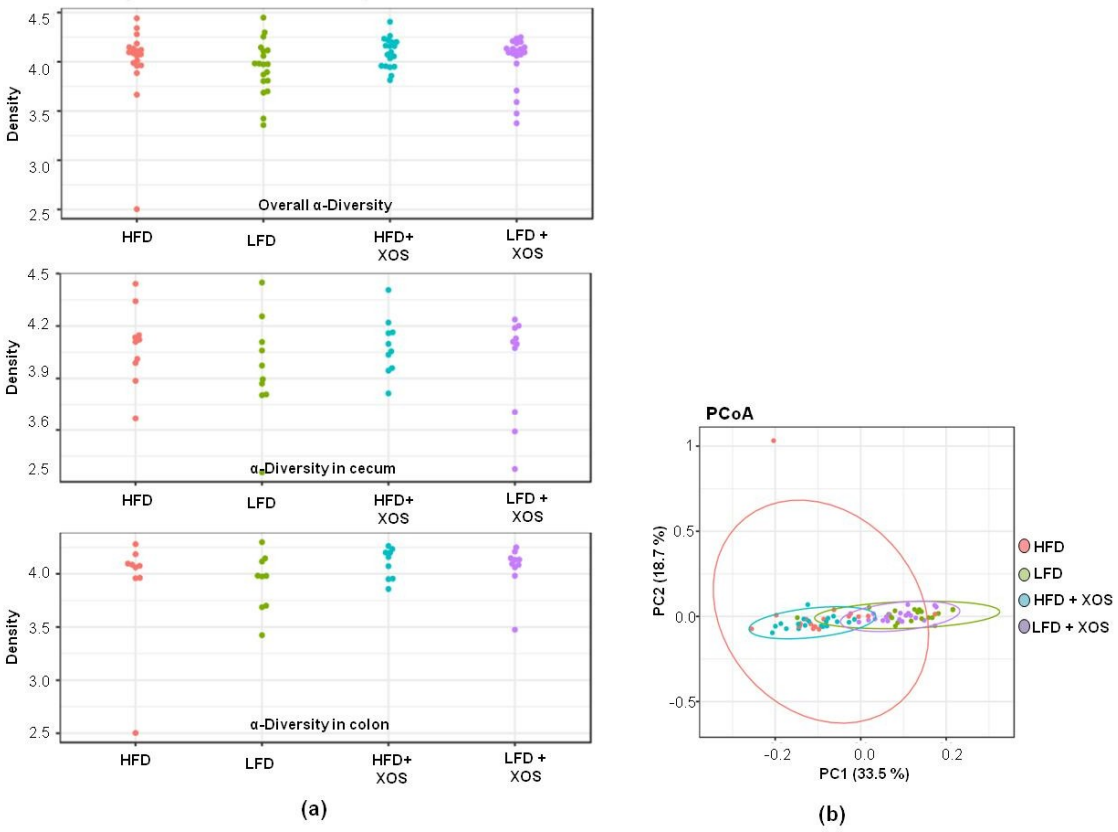

Figure 3. No significant association was observed between the diet and gut microbiota diversity. (a) The overall alpha-diversity (on top), alpha-diversity in colon (at middle) and caecum (on bottom) of the gut microbiota. The alpha-diversity of the gut microbiota was quantified with Shannon index using microbiome R/Bioconductor package; **(b)** Beta-diversity of the gut microbiota. The beta-diversity analysis was based on Bray-Curtis distance and PERMANOVA was used for significance testing (adonis function in the vegan R package).

Preprints (www.preprints.org) | NOT PEER-REVIEWED | Posted: 11 September 2020 doi:10.20944/preprints202009.0241.v1

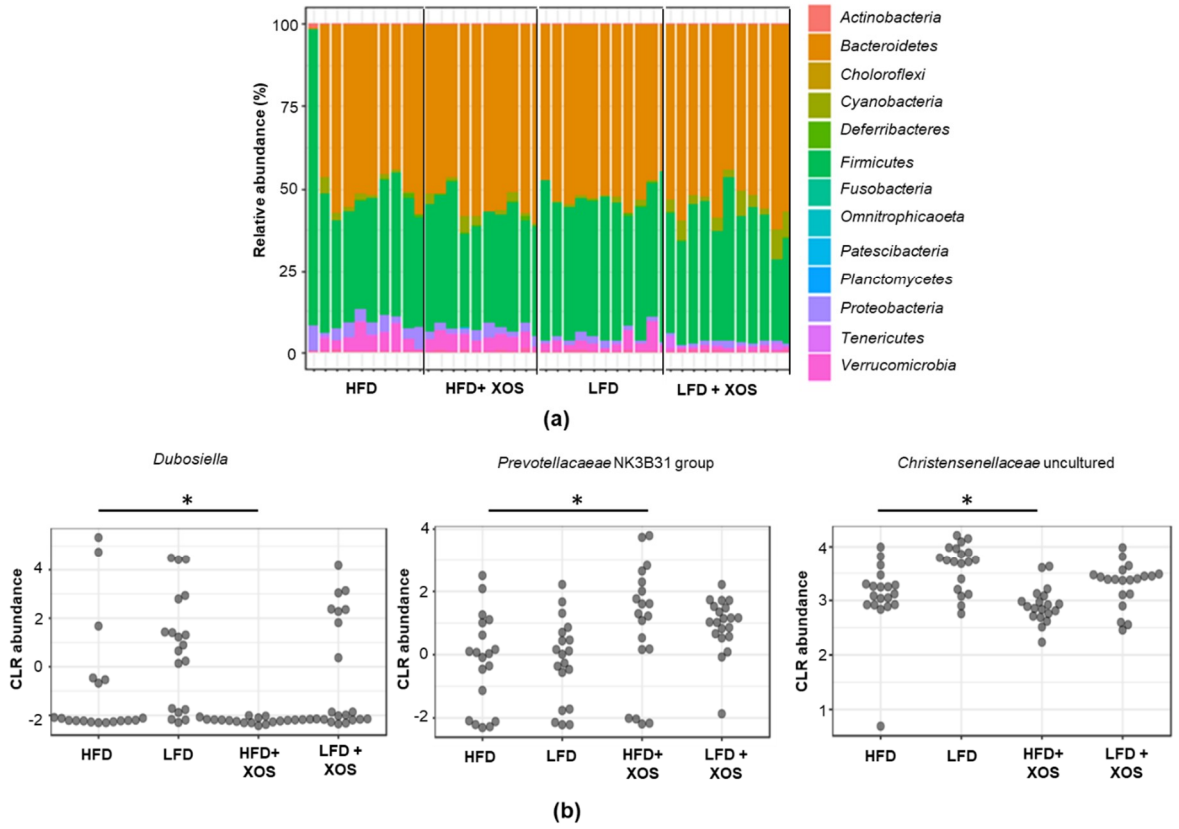

Figure 4. Differences were found in the abundance of three genera between the diet groups. (a) The gut microbiota composition of the rats at phylum level did not differ between the groups. The taxonomic groups were compared based on DESeq2 using *phyloseq* R/Bioconductor package including Benjamini-Hochberg correction for multiple testing. B) Differences between the groups were found in the abundance of *Dubosiella*, *Prevotellaceae* NK3B31 and uncultured *Christensenellaceae*. The taxonomic groups were compared based on DESeq2 using *phyloseq* R/Bioconductor package including Benjamini-Hochberg correction for multiple testing. CLR abundance = centered log-ratio transformed abundance. * indicates statistically significant difference between the groups.

3.3. Increased abundance of F. prausnitzii in the HFD+XOS group was not associated with changes in intestinal tight junctions or systemic inflammation

Due to that HFD is known to compromise gut integrity and conversely, prebiotic nutrients to enhance it, we analyzed the expression of Tjp1 in the proximal colon. The histological analysis of the tight-junctions showed no differences between the groups (Figure 5).

As mentioned, *F. prausnitzii* is reported to exert several anti-inflammatory function and therefore we were interested in studying whether its' increased abundance was associated with decreased systemic inflammation. Of the nine cytokines that were analyzed, only three were detected in rats, namely IL-10, IL-12 and TNFα. XOS supplementation and thus higher abundance of *F. prausnitzii* did not affect the levels of any of the three cytokines (Figure 6). TNFα was under the detection limit, i.e. < 2.72 pg/ml in the HFD groups, and was detected in three rats out of ten in the LFD groups, and thus the difference compared to the HFD groups did not reach statistical significance. Compared to the HFD+XOS, LFD+XOS had higher levels of anti-inflammatory IL-10 ($p=0.002$, Figure 6), and the LFD higher than the HFD ($p=0.006$, Figure 6).

Preprints (www.preprints.org) | NOT PEER-REVIEWED | Posted: 11 September 2020 doi:10.20944/preprints202009.0241.v1

3.4. The LFD improved caecal SCFA profile and on the HFD, XOS decreased caecal isovalerate and tyrosine levels

An OPLS-DA showed a clear separation between the HFD and LFD based on the component t[1] (Supplementary figure S1A). The model represented a high goodness of fit ($R^2X_{(cum)}$= 0.552 and $R^2Y_{(cum)}$= 0.9), and optimum predictive ability (Q^2= 0.841). The metabolites responsible for the separation of the HFD and LFD were identified by combining the information from S-loading plot (Figure S1B), column loading plot and Variable Importance in Projection (VIP) data. The details and comparisons are compiled in the Supplementary tables 1 and 2. The unsupervised PCA did not differentiate between the HFD and HFD+XOS (Figure S2) or between the LFD and LFD+XOS (Figure S3). The LFD was characterized by higher caecal levels of SCFAs (Table 1). The dietary fat mostly explained the clustering of the metabolites (Figure 7a). The HFD+XOS differed from the HFD by having lower caecal tyrosine (p=0.015) levels (Figure 7b). In general, XOS lowered cecal tyrosine level [F (1, 36) = 7.7, p = 0.009]. XOS and diet had an interactive effect on isovalerate [F (1, 36) = 6.0, p= 0.012] being the level of isovalerate increased with LFD and decreased with HFD (Figure 7b). Several caecal metabolites, including the SCFAs associated negatively with hepatic triglycerides (Figure 7c). Metabolites that are known to boost oxidative metabolism, such as nicotinate, butyrate and 2-oxoglutarate positively associated with the hepatic oxidative phosphorylation and negatively with triglyceride content (Figure 7c). The group-wise comparisons of the metabolites are shown in Figure S4.

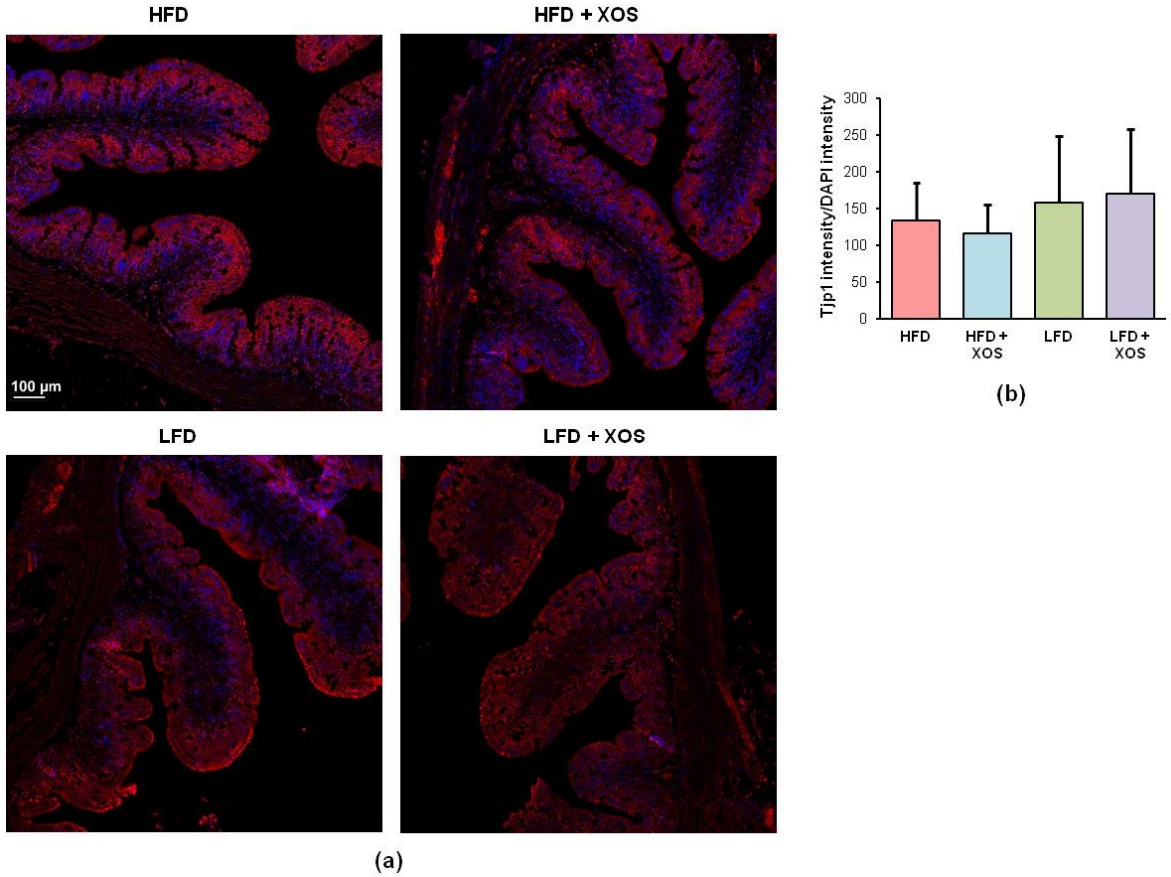

Figure 5. Intestinal Tjp1 did not differ between the diet groups. (a) The histological images were taken with Zeiss LSM 700 and 20x Plan-Apochromat 20x/0.8 M27 objective. Tjp1 is shown with red label and DAPI in blue. The scale bar is 100 µM; **(b)** The bars in the graph represent the expression of Tjp1 counted as its intensity using Image J adjusted to the intensity of DAPI.

Preprints (www.preprints.org) | NOT PEER-REVIEWED | Posted: 11 September 2020 doi:10.20944/preprints202009.0241.v1

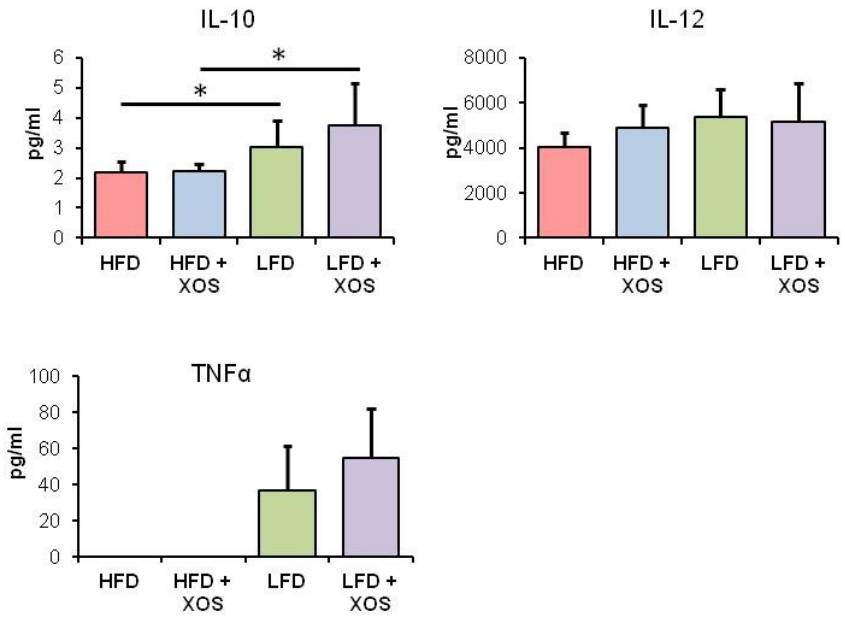

Figure 6. XOS supplementation did not affect the serum levels of IL-10, IL-12 or TNFα but the LFD groups had higher levels of anti-inflammatory IL-10. Compared to the HFD+XOS, LFD+XOS had higher levels of anti-inflammatory IL-10 as did the LFD compared to HFD. Serum cytokines were analyzed after 12-weeks of diet intervention using 9-plex ELISA, Quansys and Q-View software. Out of nine cytokines, only the levels of three were detactable in rats. * indicates statistically significant difference between the groups.

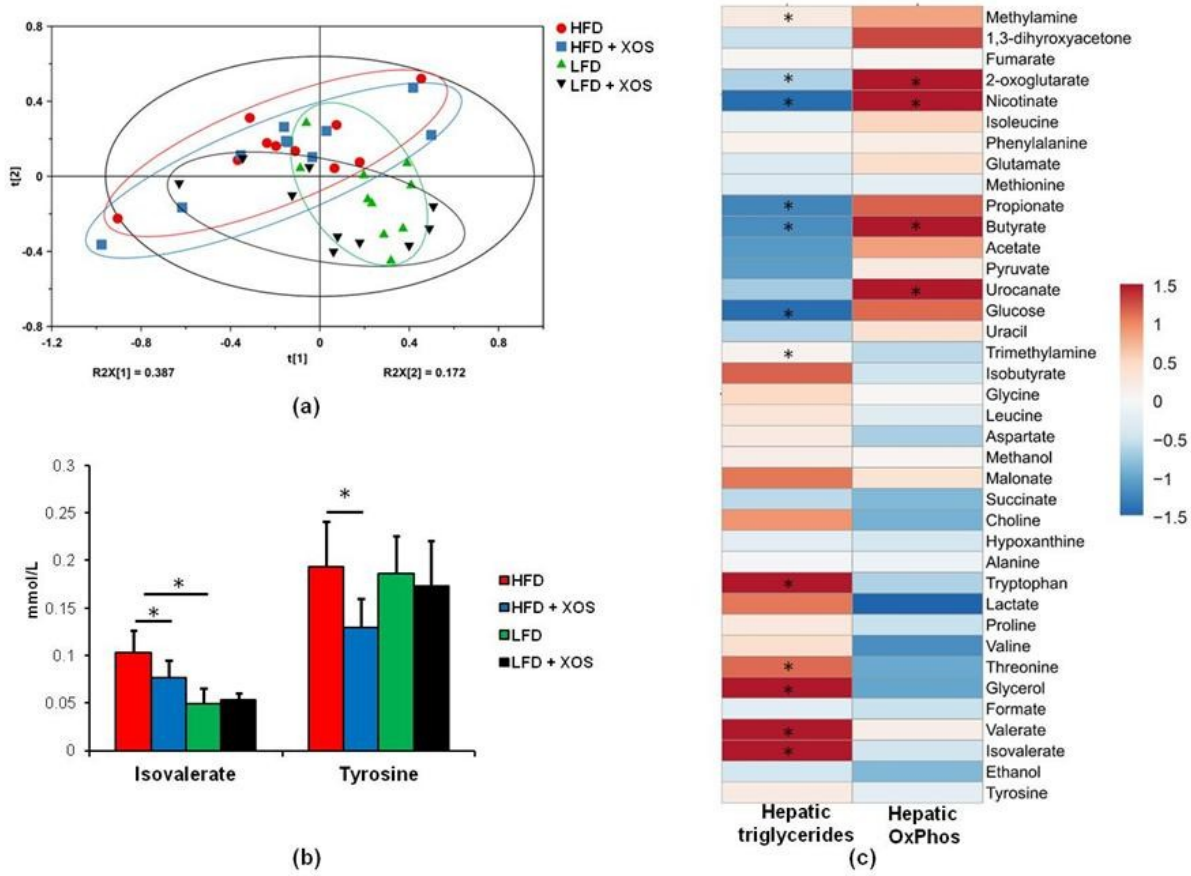

Figure 7. Compared to the HFD, HFD+XOS had decreased levels of caecal tyrosine and isovalerate. (a) Score scatter plot of the Principal Component Analysis (PCA) of caecal metabolites

Preprints (www.preprints.org) | NOT PEER-REVIEWED | Posted: 11 September 2020 doi:10.20944/preprints202009.0241.v1

shows no major differences between the groups; **(b)** Tyrosine and isovalerate levels differed between the groups. * p<0.05, **** p<0.0001; **(c)** Associations of the metabolites with the hepatic triglyceride content and oxidative phosphorylation. The heatmap was drawn using Clustvis, a web tool for visualizing clustering of multivariate data (https://biit.cs.ut.ee/clustvis/). * indicates significant association between the variables. The colored scale bar is shown on the right, the color in the figure corresponds to Spearman correlation coefficient.

Table 1. SCFA concentrations (mM, mean ± SEM) and acetate (A) : propionate (P) : butyrate (B) ratio in cecum.

Group	Acetate (A)	Propionate (P)	Butyrate (B)	Ratio A:P:B
HFD	16 ± 1.2	3.4 ± 0.22	0.91 ± 0.16	79:16:5
HFD+XOS	16 ± 1.4	3.4 ± 0.29	0.96 ± 0.13	79:16:5
LFD	22 ± 0.99	5.2 ± 0.22	2.6 ± 0.39	74:17:9
LFD+XOS	20 ± 1.2	4.9 ± 0.26	3.0 ± 0.41	72:17:11

3.5. Compared to the LFD, HFD decreased energy expenditure in rats while diet and XOS had interactive effect on energy expenditure

The HFD lowered the average energy expenditure independent of the time of day [main effect of diet: daytime, $F(1, 36) = 19.5$, $p < 0.001$; night, $F(1, 35) = 20.9$, $p < 0.001$; Figure 8a]. XOS and diet had significant interactive effect on the night time lowest resting energy expenditure [$F(1, 35) = 7.9$, $p = 0.008$] and the tendency was similar during daytime [$F(1, 36) = 3.5$, $p = 0.071$, Figure 8b]. That is, at night HFD lowered resting energy expenditure but XOS enhanced it, whereas in LFD, XOS diminished resting energy expenditure. Compared with the HFD, LFD had higher measured lowest, diurnal energy expenditure during 30 minutes ($p=0.001$, Figure 8b). At night time, the LFD had higher average energy expenditure than the HFD ($p=0.01$, Figure 8a). Consequently, the mean produced CO_2 was higher in the LFD than HFD during daytime ($p<0.001$) and at night ($p = 0.001$, Figure 8c). HFD diminished CO_2 production at night time the [$F(1, 36) = 198.5$, $p < 0.001$] and during daytime [$F(1, 34) = 164.7$, $p < 0.001$ Figure 8c]. Further, the diet had significant effect on all measured diurnal and nocturnal RQs, being the RQ values higher in the LFD than in HFD groups. The group differences are shown in the Figure 8d. In addition, the interactive effect of XOS and diet was significant on RQs on daytime and nighttime ($p<0.001$ for all, Figure 8d).

3.6. HFD+XOS did not modulate serum clinical variables or body composition compared to the HFD

Independent of the supplementation, the LFD groups weighed less than HFD during the diet intervention (Figure S5). Compared to the HFD, XOS did not affect serum levels of triglycerides, free fatty acids, total cholesterol, LDL, HDL, glycerol, AST or ALT (Figure S6). Neither did XOS influence body fat %, total fat mass, total tissue mass or the amount of epidymal or mesenteric fat, that were affected by the HFD. The LFD had lower serum glycerol ($p=0.001$) and ALT levels ($p<0.001$) than the HFD (Figure S6 & S7). The LFD also had lower body fat % ($p=0.024$), total fat mass ($p=0.001$), tissue mass ($p<0.001$), as well as epidymal ($p<0.001$) and mesenteric ($p=0.008$) fat mass than the HFD (Figure S7). Compared to the HFD+XOS, LFD+XOS had lower levels of serum glycerol ($p=0.003$), and ALT ($p<0.001$, as well as lower total fat mass ($p=0.001$) and tissue mass ($p<0.001$) (Figure S6 & S7). XOS and HFD had an interactive effect on the daily energy intake: XOS enhanced the energy intake in the HFD and diminished the energy intake in the LFD ($p=0.002$) (Figure S8).

Preprints (www.preprints.org) | NOT PEER-REVIEWED | Posted: 11 September 2020 doi:10.20944/preprints202009.0241.v1

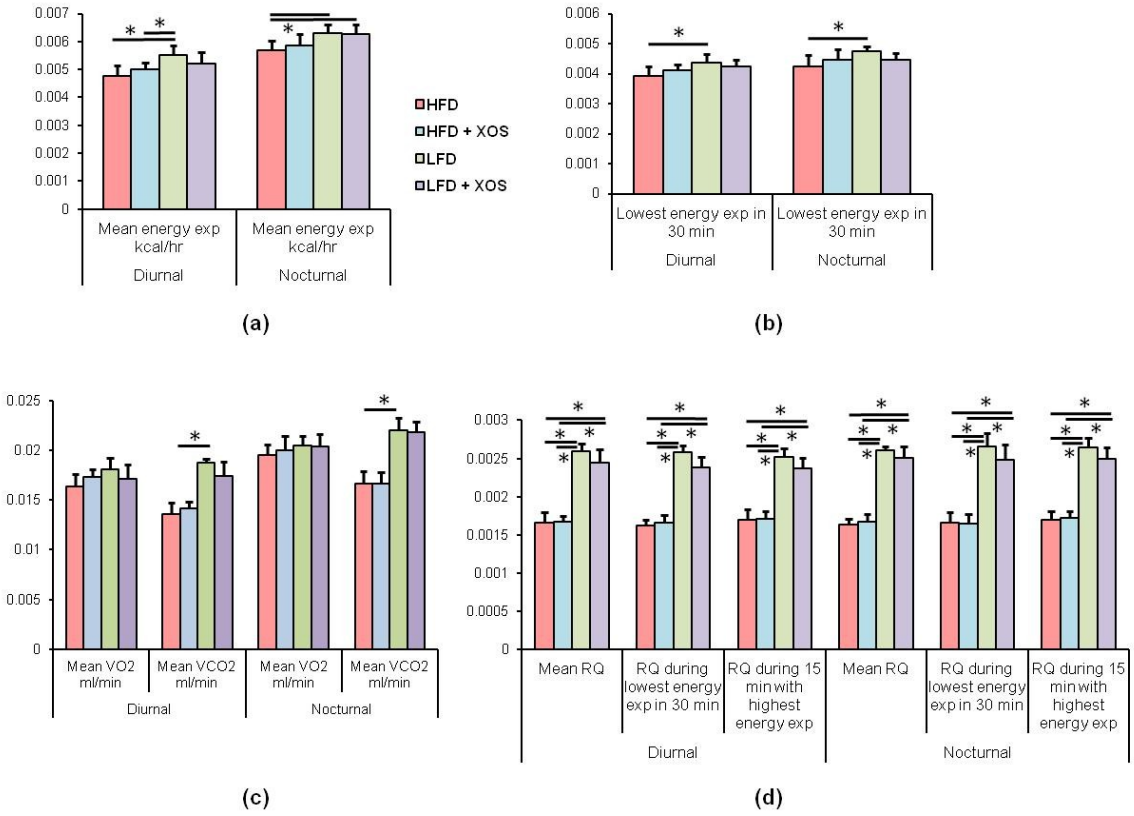

Figure 8. Compared to the HFD, LFD increased increase energy expenditure in rats, while XOS and diet had interactive effect of resipiratory quotient. **(a)** The average hourly energy expenditure was highest at night time in the LFD; **(b)** but also the lowest measured energy expenditure was highest in the LFD at day time; **(c)** HFD diminished production of CO_2 at day time, whereas in O_2 consumption no differences between the groups were found; **(d)** Respiratory Quotient (RQ) values were counted as VCO_2/VO_2. * indicates statistically significant difference ($p < 0.05$) between the groups.

4. Discussion

In this study we show that NAFLD induced by high-fat diet in rats could be partly treated by targeting gut microbiota with dietary, prebiotic Xylo-oligosaccharides (XOS). We show that prebiotic diet increased both *in vitro* and *in vivo* the abundance of *Faecalibacterium prausnitzii,* whose low relative abundance has been associated with high hepatic fat content in humans [24]. Here we challenged the rats with high fat diet or not, and with XOS supplementation or not. The hepatic fat and triglyceride contents were diminished in the XOS-supplemented high fat diet group, by the XOS enhancing hepatic β-oxidation and mitochondrial respiration. Our own previous study in a mice model suggested that NAFLD could be alleviated with administering intragastrically *F. prausnitzii* [23]. Previously, XOS has been shown to have prebiotic properties by supporting the abundance of beneficial bacteria, such as *Lactobacilli* and *Bifidobacteria* as well as *Faecalibacterium* species [36]. Yet, explicitly *F. prausnitzii* was not studied. In contrast to our present findings, by studying bacteria in a human colonic simulator, Christophersen *et al.* found that XOS decreased the growth of *F. prausnitzii* [28], which is considered as one potential next generation probiotic bacterium [37].

 doi:10.20944/preprints202009.0241.v1

Besides the increase in *F. prausnitzii* abundance, surprisingly small changes in the GM composition of rats occurred in response to 12-week XOS-supplementation, and no changes in the integrity of gut epithelia were observed in any of the groups as revealed by immunohistological staining of intestinal tight junctions. The latter finding was somewhat surprising because we have earlier shown that *F. prausnitzii* administration increased intestinal *Tjp1* mRNA expression [23], and others have shown that prebiotic oligosaccharides in general can prevent HFD-induced impairment of gut permeability [38]. Independent of the dietary fat, XOS increased the abundance of *Prevotellacaeae* NK3B31 group in rats. Similarly, others have shown that increasing dietary fiber by pectin supplementation, the abundance of this bacterial group increased in rats [39]. To our knowledge, *Prevotellacaeae* NK3B31 has not been linked before to NAFLD. It has been shown to negatively associate with serum triglycerides and LDL cholesterol in type 2 diabetic rats [40] that, however, are frequently associated with NAFLD. *Prevotella* may be involved in host's fat metabolism, likely through SCFAs, that they are known to produce from dietary fibers [41]. Yet, we did not detect higher levels of caecal SCFAs in the XOS-supplemented rats. *Dubosiella* and an uncultured member of *Christensenellaceae* were as high in the LFD groups as in the HFD group without XOS supplementation. These were rather unexpected findings, because an obese human cohort has shown a decreased relative abundance of *Christensenellaceae* [42], and a member of this family, *Christensenella minuta* has been suggested to promote lean host phenotype [43]. However, interestingly in our study, XOS supplementation decreased the abundance of *Christensenellaceae* in the HFD group.

Despite the increase in the abundance of *F. prausnitzii* that is considered an important anti-inflammatory bacterium [21, 22], no differences in serum cytokines IL-10, IL-12 or TNFα were found in response to XOS supplementation. However, interestingly, compared to the HFD+XOS, LFD+XOS had higher serum levels and LFD higher than HFD of anti-inflammatory IL-10. This result is in agreement with lower levels of IL-10 in NAFLD patients and higher levels in healthy controls [44].

Of the prebiotic fibers, alpha-galacto-oligosaccharides [45] and fructo-oligosaccharides [46] have been shown to improve NAFLD in preclinical models, but to the best of our knowledge this study is the first to describe such effect for XOS. Concomitantly with the increase in *F. prausnitzii*, XOS decreased the content of hepatic triglycerides in HFD fed rats. This was explained by the XOS enhancing the activity of hepatic β-HAD, mitochondrial respiratory capacity available for ATP production through electron flow from complex I, coupling of electron transport through complex I, and oxidative phosphorylation. β-HAD is a subunit of the mitochondrial trifunctional enzyme subunit alpha (MTP), which catalyzes the last three steps of fatty acid β-oxidation. Previously, heterozygous $MTP^{+/-}$ mice were shown to develop NAFLD simultaneously with a reduced rate of β-oxidation [47], thus, highlighting the importance of MTP in the onset of the disease. The enhanced β-oxidation, glucose oxidation and mitochondrial respiration in our study may be interrelated through the shared substrates or because MTP can directly interact with the NADH-binding domain of complex I of the electron transfer chain [48].

Despite the improvements in hepatic metabolism, diet or XOS caused surprisingly small effects on the whole body energy expenditure and respiratory quotient. However, as expected, the HFD enhanced caloric intake, body weight gain and fat content compared to the LFD. Nevertheless, it is a limitation that we studied here only the metabolic differences between the diurnal and nocturnal periods, and more detailed analyses throughout the day might be needed to get more insight into the energy metabolism.

On the HFD, XOS diminished the levels of caecal metabolites tyrosine and isovalerate, which reduction has likely contributed to the increased hepatic fat oxidation. We assume this because NASH patients have been shown to have higher levels of tyrosine [49] and dysregulated metabolism of tyrosine [50]. The consequences of the dysregulated metabolism of tyrosine are not entirely clear, but it has been proposed that tyrosine could enter the ketogenic pathway and be degraded directly to acetyl-CoA [51]. Therefore, high tyrosine might stimulate fatty acid synthesis and thus contribute to lipid deposition in liver. The XOS-induced decrease in the caecal tyrosine is possibly due to an

increased microbial metabolism of it [52], which may have contributed to the decreased hepatic fat content when less tyrosine is transported through the gut-liver-axis. The GM-produced isovalerate could also have participated in NAFLD. This view is supported by a study, in which the GM from NAFLD mice and healthy mice were transplanted into germ-free mice. The mice receiving the microbiota of the NAFLD mice had significantly higher faecal isovalerate levels [53]. In another study, faecal nicotinic acid, butyrate and 2-oxoglutarate were associated negatively with hepatic fat content and positively with oxidative phosphorylation. Behind these associations may be the capacity of nicotinic acid to inhibit fatty acid flux from adipose tissue to liver [54]. Similarly, 2-oxoglutarate and butyrate are known to promote hepatic oxidative metabolism [55]. However, in our study, XOS did not promote butyrate production and neither did it likely affect gut permeability as determined from the amount of intestinal tight junctions.

5. Conclusions

Our study provides evidence of that commensal and health-beneficial gut microbes, such as *Faecalibacterium prausnitzii* can be targeted with specific dietary supplements to ameliorate NAFLD by enhancing their natural growth in the gut. Further, we identified the enhanced hepatic oxidative metabolism and mitochondrial functions as the underlying gut microbiota and prebiotic-dependent preventive mechanisms of NAFLD. However, our study was done in rats and it should be further studied in human cohorts whether our findings on XOS improving NAFLD can be extended to humans.

Author Contributions: Conceptualization, S.L., E.M., and S.P.; methodology, S.L., R.P., E.M., W.S., E.M., A.D., B.Y., J.L., M.L., M.T., and S.P..; formal analysis, S.L., L.L., B.Y., M.T., S.P.; resources, L.L., M.T., S.P.; writing—original draft preparation, S.L., L.L:, S.P.; writing—review and editing, ALL AUTHORS; supervision, L.L., and S.P.; funding acquisition, B.Y., M.T., L.L., and S.P. All authors have read and agreed to the published version of the manuscript.

Funding: This study was financially supported by the Academy of Finland Researcher fellowship for Dr. Pekkala (Grant ID 308042) and by the ERVA funding of The Hospital District of Southwest Finland for Dr. Pekkala.

Acknowledgments: We thank Eliisa Kiukkanen for the animal care and maintenance. We thank Sanja Vanhatalo for the help in *Faecalibacterium prausnitzii* cultures. Anniina Keskitalo is thanked for preparing the *F. prausnitzii* standard curve for qPCR. We thank Mervi Matero, Hanne Tähti, Jukka Hintikka, Elina Virtanen and Markus Honkanen for the excellent technical assistance.

Conflicts of Interest: The authors declare no conflict of interest. The funders had no role in the design of the study; in the collection, analyses, or interpretation of data; in the writing of the manuscript, or in the decision to publish the results.

References

1. Araujo, A.R., N. Rosso, G. Bedogni, C. Tiribelli, and S. Bellentani, Global epidemiology of non-alcoholic fatty liver disease/non-alcoholic steatohepatitis: What we need in the future. *Liver Int,* **2018**. 38 Suppl 1: p. 47-51.
2. Wong, V.W., G.L. Wong, P.C. Choi, A.W. Chan, M.K. Li, H.Y. Chan, A.M. Chim, J. Yu, J.J. Sung, and H.L. Chan, Disease progression of non-alcoholic fatty liver disease: a prospective study with paired liver biopsies at 3 years. *Gut,* **2010**. 59(7): p. 969-74.
3. McPherson, S., T. Hardy, E. Henderson, A.D. Burt, C.P. Day, and Q.M. Anstee, Evidence of NAFLD progression from steatosis to fibrosing-steatohepatitis using paired biopsies: implications for prognosis and clinical management. *J Hepatol,* **2015**. 62(5): p. 1148-55.

4. Tilg, H. and A.R. Moschen, Evolution of inflammation in nonalcoholic fatty liver disease: the multiple parallel hits hypothesis. *Hepatology*, **2010**. 52(5): p. 1836-46.
5. Ozcan, L., A.S. Ergin, A. Lu, J. Chung, S. Sarkar, D. Nie, M.G. Myers, Jr., and U. Ozcan, Endoplasmic reticulum stress plays a central role in development of leptin resistance. *Cell Metab*, **2009**. 9(1): p. 35-51.
6. Sha, H., Y. He, H. Chen, C. Wang, A. Zenno, H. Shi, X. Yang, X. Zhang, and L. Qi, The IRE1alpha-XBP1 pathway of the unfolded protein response is required for adipogenesis. *Cell Metab*, **2009**. 9(6): p. 556-64.
7. Begriche, K., J. Massart, M.A. Robin, F. Bonnet, and B. Fromenty, Mitochondrial adaptations and dysfunctions in nonalcoholic fatty liver disease. *Hepatology*, **2013**. 58(4): p. 1497-507.
8. Zmora, N., J. Suez, and E. Elinav, You are what you eat: diet, health and the gut microbiota. *Nat Rev Gastroenterol Hepatol*, **2019**. 16(1): p. 35-56.
9. Henao-Mejia, J., E. Elinav, C.A. Thaiss, P. Licona-Limon, and R.A. Flavell, Role of the intestinal microbiome in liver disease. *J Autoimmun*, **2013**. 46: p. 66-73.
10. Henao-Mejia, J., E. Elinav, C.A. Thaiss, and R.A. Flavell, The intestinal microbiota in chronic liver disease. *Adv Immunol*, **2013**. 117: p. 73-97.
11. Spencer, M.D., T.J. Hamp, R.W. Reid, L.M. Fischer, S.H. Zeisel, and A.A. Fodor, Association between composition of the human gastrointestinal microbiome and development of fatty liver with choline deficiency. *Gastroenterology*, **2011**. 140(3): p. 976-86.
12. Michail, S., M. Lin, M.R. Frey, R. Fanter, O. Paliy, B. Hilbush, and N.V. Reo, Altered gut microbial energy and metabolism in children with non-alcoholic fatty liver disease. *FEMS Microbiol Ecol*, **2015**. 91(2): p. 1-9.
13. Raman, M., I. Ahmed, P.M. Gillevet, C.S. Probert, N.M. Ratcliffe, S. Smith, R. Greenwood, M. Sikaroodi, V. Lam, P. Crotty, J. Bailey, R.P. Myers, and K.P. Rioux, Fecal microbiome and volatile organic compound metabolome in obese humans with nonalcoholic fatty liver disease. *Clin Gastroenterol Hepatol*, **2013**. 11(7): p. 868-75 e1-3.
14. Mouzaki, M., E.M. Comelli, B.M. Arendt, J. Bonengel, S.K. Fung, S.E. Fischer, I.D. McGilvray, and J.P. Allard, Intestinal microbiota in patients with nonalcoholic fatty liver disease. *Hepatology*, **2013**. 58(1): p. 120-7.
15. Zhu, L., S.S. Baker, C. Gill, W. Liu, R. Alkhouri, R.D. Baker, and S.R. Gill, Characterization of gut microbiomes in nonalcoholic steatohepatitis (NASH) patients: a connection between endogenous alcohol and NASH. *Hepatology*, **2013**. 57(2): p. 601-9.
16. Shen, F., R.D. Zheng, X.Q. Sun, W.J. Ding, X.Y. Wang, and J.G. Fan, Gut microbiota dysbiosis in patients with non-alcoholic fatty liver disease. *Hepatobiliary Pancreat Dis Int*, **2017**. 16(4): p. 375-381.
17. Suzuki, T.A. and M. Worobey, Geographical variation of human gut microbial composition. *Biol Lett*, **2014**. 10(2): p. 20131037.
18. O'Toole, P.W. and I.B. Jeffery, Gut microbiota and aging. *Science*, **2015**. 350(6265): p. 1214-5.
19. Mariat, D., O. Firmesse, F. Levenez, V. Guimaraes, H. Sokol, J. Dore, G. Corthier, and J.P. Furet, The Firmicutes/Bacteroidetes ratio of the human microbiota changes with age. *BMC Microbiol*, **2009**. 9: p. 123.
20. Haro, C., O.A. Rangel-Zuniga, J.F. Alcala-Diaz, F. Gomez-Delgado, P. Perez-Martinez, J. Delgado-Lista, G.M. Quintana-Navarro, B.B. Landa, J.A. Navas-Cortes, M. Tena-Sempere, J.C. Clemente, J. Lopez-Miranda, F. Perez-Jimenez, and A. Camargo, Intestinal Microbiota Is Influenced by Gender and Body Mass Index. *PLoS One*, **2016**. 11(5): p. e0154090.

21. Miquel, S., M. Leclerc, R. Martin, F. Chain, M. Lenoir, S. Raguideau, S. Hudault, C. Bridonneau, T. Northen, B. Bowen, L.G. Bermudez-Humaran, H. Sokol, M. Thomas, and P. Langella, Identification of metabolic signatures linked to anti-inflammatory effects of Faecalibacterium prausnitzii. *MBio,* **2015**. 6(2).
22. Quevrain, E., M.A. Maubert, C. Michon, F. Chain, R. Marquant, J. Tailhades, S. Miquel, L. Carlier, L.G. Bermudez-Humaran, B. Pigneur, O. Lequin, P. Kharrat, G. Thomas, D. Rainteau, C. Aubry, N. Breyner, C. Afonso, S. Lavielle, J.P. Grill, G. Chassaing, J.M. Chatel, G. Trugnan, R. Xavier, P. Langella, H. Sokol, and P. Seksik, Identification of an anti-inflammatory protein from Faecalibacterium prausnitzii, a commensal bacterium deficient in Crohn's disease. *Gut,* **2016**. 65(3): p. 415-25.
23. Munukka, E., A. Rintala, R. Toivonen, M. Nylund, B. Yang, A. Takanen, A. Hanninen, J. Vuopio, P. Huovinen, S. Jalkanen, and S. Pekkala, Faecalibacterium prausnitzii treatment improves hepatic health and reduces adipose tissue inflammation in high-fat fed mice. *ISME J,* **2017**.
24. Munukka, E., S. Pekkala, P. Wiklund, O. Rasool, R. Borra, L. Kong, X. Ojanen, S.M. Cheng, C. Roos, S. Tuomela, M. Alen, R. Lahesmaa, and S. Cheng, Gut-adipose tissue axis in hepatic fat accumulation in humans. *J Hepatol,* **2014**. 61(1): p. 132-8.
25. Wong, V.W., C.H. Tse, T.T. Lam, G.L. Wong, A.M. Chim, W.C. Chu, D.K. Yeung, P.T. Law, H.S. Kwan, J. Yu, J.J. Sung, and H.L. Chan, Molecular characterization of the fecal microbiota in patients with nonalcoholic steatohepatitis--a longitudinal study. *PLoS One,* **2013**. 8(4): p. e62885.
26. Markowiak, P. and K. Slizewska, Effects of Probiotics, Prebiotics, and Synbiotics on Human Health. *Nutrients,* **2017**. 9(9).
27. Finegold, S.M., Z. Li, P.H. Summanen, J. Downes, G. Thames, K. Corbett, S. Dowd, M. Krak, and D. Heber, Xylooligosaccharide increases bifidobacteria but not lactobacilli in human gut microbiota. *Food Funct,* **2014**. 5(3): p. 436-45.
28. Christophersen, C.T., A. Petersen, T.R. Licht, and M.A. Conlon, Xylo-oligosaccharides and inulin affect genotoxicity and bacterial populations differently in a human colonic simulator challenged with soy protein. *Nutrients,* **2013**. 5(9): p. 3740-56.
29. Scott, K.P., J.C. Martin, S.H. Duncan, and H.J. Flint, Prebiotic stimulation of human colonic butyrate-producing bacteria and bifidobacteria, in vitro. *FEMS Microbiol Ecol,* **2014**. 87(1): p. 30-40.
30. Yang, J., P.H. Summanen, S.M. Henning, M. Hsu, H. Lam, J. Huang, C.H. Tseng, S.E. Dowd, S.M. Finegold, D. Heber, and Z. Li, Xylooligosaccharide supplementation alters gut bacteria in both healthy and prediabetic adults: a pilot study. *Front Physiol,* **2015**. 6: p. 216.
31. Cunningham, J.J., Calculation of energy expenditure from indirect calorimetry: assessment of the Weir equation. *Nutrition,* **1990**. 6(3): p. 222-3.
32. Sokol, H., P. Seksik, J.P. Furet, O. Firmesse, I. Nion-Larmurier, L. Beaugerie, J. Cosnes, G. Corthier, P. Marteau, and J. Dore, Low counts of Faecalibacterium prausnitzii in colitis microbiota. *Inflamm Bowel Dis,* **2009**. 15(8): p. 1183-9.
33. Toivonen R, V.S., Hollmén M, Munukka E, Keskitalo A, Pietilä S, Elo L, Huovinen P, Jalkanen S, Pekkala S., Vascular Adhesion Protein 1 Mediates Gut Microbial Flagellin-Induced Inflammation, Leukocyte Infiltration, and Hepatic Steatosis. *Sci,* **2019**.
34. Kelly, B.J., R. Gross, K. Bittinger, S. Sherrill-Mix, J.D. Lewis, R.G. Collman, F.D. Bushman, and H. Li, Power and sample-size estimation for microbiome studies using pairwise distances and PERMANOVA. *Bioinformatics,* **2015**. 31(15): p. 2461-8.

35. Love, M.I., W. Huber, and S. Anders, Moderated estimation of fold change and dispersion for RNA-seq data with DESeq2. *Genome Biol,* **2014**. 15(12): p. 550.
36. Lin, S.H., L.M. Chou, Y.W. Chien, J.S. Chang, and C.I. Lin, Prebiotic Effects of Xylooligosaccharides on the Improvement of Microbiota Balance in Human Subjects. *Gastroenterol Res Pract,* **2016**. 2016: p. 5789232.
37. Langella, P., F. Guarner, and R. Martin, Editorial: Next-Generation Probiotics: From Commensal Bacteria to Novel Drugs and Food Supplements. *Front Microbiol,* **2019**. 10: p. 1973.
38. Hamilton, M.K., C.C. Ronveaux, B.M. Rust, J.W. Newman, M. Hawley, D. Barile, D.A. Mills, and H.E. Raybould, Prebiotic milk oligosaccharides prevent development of obese phenotype, impairment of gut permeability, and microbial dysbiosis in high fat-fed mice. *Am J Physiol Gastrointest Liver Physiol,* **2017**. 312(5): p. G474-G487.
39. Ferrario, C., R. Statello, L. Carnevali, L. Mancabelli, C. Milani, M. Mangifesta, S. Duranti, G.A. Lugli, B. Jimenez, S. Lodge, A. Viappiani, G. Alessandri, M. Dall'Asta, D. Del Rio, A. Sgoifo, D. van Sinderen, M. Ventura, and F. Turroni, How to Feed the Mammalian Gut Microbiota: Bacterial and Metabolic Modulation by Dietary Fibers. *Front Microbiol,* **2017**. 8: p. 1749.
40. Wei, X., J. Tao, S. Xiao, S. Jiang, E. Shang, Z. Zhu, D. Qian, and J. Duan, Xiexin Tang improves the symptom of type 2 diabetic rats by modulation of the gut microbiota. *Sci Rep,* **2018**. 8(1): p. 3685.
41. Koh, A., F. De Vadder, P. Kovatcheva-Datchary, and F. Backhed, From Dietary Fiber to Host Physiology: Short-Chain Fatty Acids as Key Bacterial Metabolites. *Cell,* **2016**. 165(6): p. 1332-1345.
42. Peters, B.A., J.A. Shapiro, T.R. Church, G. Miller, C. Trinh-Shevrin, E. Yuen, C. Friedlander, R.B. Hayes, and J. Ahn, A taxonomic signature of obesity in a large study of American adults. *Sci Rep,* **2018**. 8(1): p. 9749.
43. Goodrich, J.K., J.L. Waters, A.C. Poole, J.L. Sutter, O. Koren, R. Blekhman, M. Beaumont, W. Van Treuren, R. Knight, J.T. Bell, T.D. Spector, A.G. Clark, and R.E. Ley, Human genetics shape the gut microbiome. *Cell,* **2014**. 159(4): p. 789-99.
44. Zahran, W.E., K.A. Salah El-Dien, P.G. Kamel, and A.S. El-Sawaby, Efficacy of Tumor Necrosis Factor and Interleukin-10 Analysis in the Follow-up of Nonalcoholic Fatty Liver Disease Progression. *Indian J Clin Biochem,* **2013**. 28(2): p. 141-6.
45. Chappuis, E., F. Morel-Depeisse, B. Bariohay, and J. Roux, Alpha-Galacto-Oligosaccharides at Low Dose Improve Liver Steatosis in a High-Fat Diet Mouse Model. *Molecules,* **2017**. 22(10).
46. Yao, F., R. Jia, H. Huang, Y. Yu, L. Mei, L. Bai, Y. Ding, and P. Zheng, Effect of Lactobacillus paracasei N1115 and fructooligosaccharides in nonalcoholic fatty liver disease. *Arch Med Sci,* **2019**. 15(5): p. 1336-1344.
47. Rector, R.S., E.M. Morris, S. Ridenhour, G.M. Meers, F.F. Hsu, J. Turk, and J.A. Ibdah, Selective hepatic insulin resistance in a murine model heterozygous for a mitochondrial trifunctional protein defect. *Hepatology,* **2013**. 57(6): p. 2213-23.
48. Wang, Y., J. Palmfeldt, N. Gregersen, A.M. Makhov, J.F. Conway, M. Wang, S.P. McCalley, S. Basu, H. Alharbi, C. St Croix, M.J. Calderon, S. Watkins, and J. Vockley, Mitochondrial fatty acid oxidation and the electron transport chain comprise a multifunctional mitochondrial protein complex. *J Biol Chem,* **2019**. 294(33): p. 12380-12391.
49. Gitto, S., F. Schepis, P. Andreone, and E. Villa, Study of the Serum Metabolomic Profile in Nonalcoholic Fatty Liver Disease: Research and Clinical Perspectives. *Metabolites,* **2018**. 8(1).

 doi:10.20944/preprints202009.0241.v1

50. Gaggini, M., F. Carli, C. Rosso, E. Buzzigoli, M. Marietti, V. Della Latta, D. Ciociaro, M.L. Abate, R. Gambino, M. Cassader, E. Bugianesi, and A. Gastaldelli, Altered amino acid concentrations in NAFLD: Impact of obesity and insulin resistance. *Hepatology,* **2018**. 67(1): p. 145-158.
51. Jin, R., S. Banton, V.T. Tran, J.V. Konomi, S. Li, D.P. Jones, and M.B. Vos, Amino Acid Metabolism is Altered in Adolescents with Nonalcoholic Fatty Liver Disease-An Untargeted, High Resolution Metabolomics Study. *J Pediatr,* **2016**. 172: p. 14-19 e5.
52. Zheng, X., G. Xie, A. Zhao, L. Zhao, C. Yao, N.H. Chiu, Z. Zhou, Y. Bao, W. Jia, J.K. Nicholson, and W. Jia, The footprints of gut microbial-mammalian co-metabolism. *J Proteome Res,* **2011**. 10(12): p. 5512-22.
53. Le Roy, T., M. Llopis, P. Lepage, A. Bruneau, S. Rabot, C. Bevilacqua, P. Martin, C. Philippe, F. Walker, A. Bado, G. Perlemuter, A.M. Cassard-Doulcier, and P. Gerard, Intestinal microbiota determines development of non-alcoholic fatty liver disease in mice. *Gut,* **2013**. 62(12): p. 1787-94.
54. Linder, K., C. Willmann, K. Kantartzis, J. Machann, F. Schick, M. Graf, S. Kummerle, H.U. Haring, A. Fritsche, N. Stefan, and R. Wagner, Dietary Niacin Intake Predicts the Decrease of Liver Fat Content During a Lifestyle Intervention. *Sci Rep,* **2019**. 9(1): p. 1303.
55. Jones, J.G., Hepatic glucose and lipid metabolism. *Diabetologia,* **2016**. 59(6): p. 1098-103.